# Chiral Interconversions of Pd and/or Au Bis-Metalated [32]Octaphyrins(1,0,1,0,1,0,1,0) Involving Hückel and Möbius Macrocyclic Topologies: A Theoretical Prediction

Zeyu Liu, Ziqi Tian, Wenbin Li, Suci Meng, Leyong Wang, and Jing Ma*

Key Laboratory of Mesoscopic Chemistry of MOE, School of Chemistry and Chemical Engineering, Nanjing University, Nanjing, 210093, People's Republic of China

Ⓢ Supporting Information

ABSTRACT: Several Pd and/or Au bis-metalated [32]-octaphyrins(1,0,1,0,1,0,1,0) were theoretically designed with rich conformations of Hückel or Möbius topology. The conformations and hence properties of macrocycles were tuned by twisting the active pyrrolic ring either clockwise (through multistep reactions with several Hückel and Möbius macrocyclic intermediates) or anticlockwise (via a direct Hückel−Hückel chiral interconversion). The encapsulated metal atoms, M_1, M_2 = Pd, Au, give different impacts on these two reaction processes. Facile occurrences of chiral interconversions between two enantiomers of bis-metalated octaphyrins were predicted with the largest activation barrier less than 40 kcal/mol. Some Au-coordinated octaphyrins (M_1 = Au) were demonstrated to be thermodynamically stable with large negative nucleus-independent chemical shift (NICS) values, which are comparable to those of the synthetic Pd-coordinated complexes. The free-base [32]octaphyrins(1,0,1,0,1,0,1,0) display the characteristic absorption spectra with distinct sharp Soret-like bands. After metalation, the Soret-like bands are red-shifted in different degrees along with the appearance of rather weak Q-like band. The heterometal-coordinated complexes (i.e., $M_1 \neq M_2$) show stronger and more splitting absorptions than the homometal-coordinated ones with $M_1 = M_2$. The hyperpolarizabilities sharply augment with the metalation in Hückel systems due to the destruction of the centrosymmetry and the increase in polarizability by coordinated metal atoms.
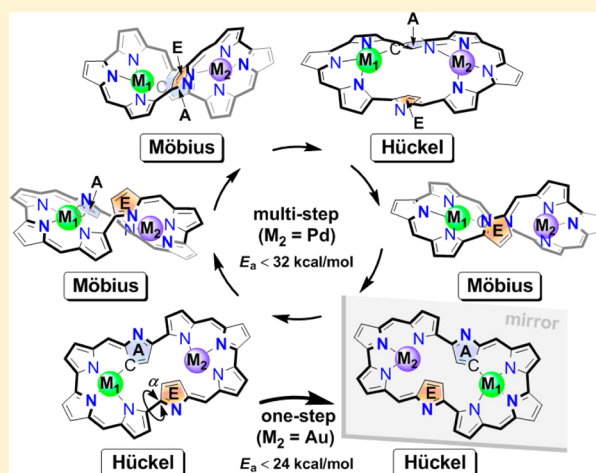
1. INTRODUCTION

Since the concept of Möbius aromaticity was proposed by Heibronner in 1964,[1] the realization of the Möbius molecules has continued to be an interesting topic in organic chemistry.[2,3] Herges and co-workers reported the first stable Möbius [16]annulene, in which the twist structure was achieved by joining the "normal" and "in-plane" π-conjugations.[4,5] However, it is still debatable whether the Möbius annulene is aromatic or not.[5−7] The requirement of simultaneous accommodation of the smoothly linked p-orbital network and the twisted molecular framework makes it rather difficult to form a stable Möbius structure. To avoid the breaking of the twisted molecule by large ring strain, metal encapsulation in the macrocycle is one of the efficient ways to stabilize the structure with novel topology, no matter whether the metalation products are aromatic or not.[8−10] Some metalated Möbius molecules including mono-Ni[II] [28]hexaphyrin, mono-Pd[II] [28]hexaphyrin, mono-Pt[II] [28]hexaphyrins, mono-Pd[II] [32]-heptaphyrin, and bis-Pd[II]/Pd[II] [36]octaphyrin have been successfully prepared by Osuka et al.[9,11,12] It has also been demonstrated that the 4n π-electron Möbius systems are more aromatic than their Hückel isomers and free-base ring in terms of various electronic and structural aromaticity criteria.[8]

On the other hand, free-base expanded porphyrins can undergo facile topological change between Hückel and Möbius isomers under suitable conditions due to their extremely flexible backbones. Latos-Grażyński and co-workers showed examples of conformational changes between topologically different states (planar Hückel, Möbius, and twisted Hückel) of di-p-benzi[28]hexaphyrin(1,1,1,1,1,1).[13,14] Osuka et al. also explored the conformational switching among a planar Hückel topology and several Möbius aromatic conformers of meso-aryl-substituted [28]hexaphyrins(1.1.1.1.1.1) in solution.[15] The synthesis of novel macrocycles, such as confusion, inversion, and fusion, have further extended the member of the prophyrin family and afforded new chances for coordination chemistry and supremolecular chemistry.[16−20] The expanded prophyrins with fascinating topology have aroused great attention due to their unique properties in NH-tautomersim, photophysics, and anion-binding.
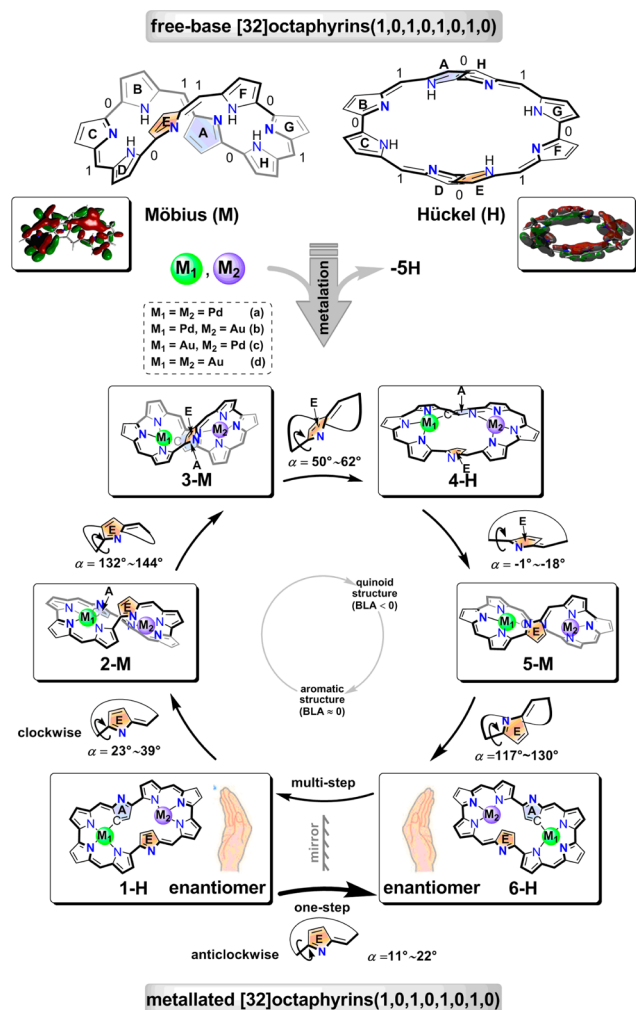
Relative to the large amount of the N-confused and N-fused porphyrins, only a few N-inversions were reported in the literature so far.[16,20] In the present work, we theoretically designed some topologically different structures of the bis-metalated [32]octaphyrins(1,0,1,0,1,0,1,0) (Scheme 1, the

Scheme 1. Free-base and Bis-metalated [32]Octaphyrins(1,0,1,0,1,0,1,0)

notation "H" and "M" denote the molecules with Hückel and Möbius topologies, respectively). There are six intermediates along the isomerization pathway, called 1-H, 2-M, 3-M, 4-H, 5-M, and 6-H. Pyrroles A and E are two inverted rings in the initial Hückel-type 1-H. The remaining pyrrolic units are named, in order, B, C, D, F, G, and H. The conformations and hence properties of macrocycles were tuned by twisting the active pyrrole E either clockwise (through multistep reactions with several Hückel and Möbius intermediates) or anticlockwise (via one-step Hückel–Hückel chiral interconversion). The adoption of "clockwise" and "anticlockwise" intends to denote two different directions of rotating the bond between pyrroles D and E (see Scheme 1 for details). The encapsulated metal atoms, M_1, M_2 = Pd, Au, give different impacts on these two reaction processes.

2. CALCULATION DETAILS

The ground-state geometries of all stationary points were fully optimized by using the B3LYP functional.[21,22] The 6-31G(d,p) basis

set for nonmetal atoms (H, C, and N) and LanL2DZ basis set for metal atoms (Pd and Au) were adopted for complexes. All stationary points were characterized as the local minima or transition structures by vibrational frequency calculations. The zero-point energy (ZPE) corrections were taken into account for relative energy. The NICS values at the center of macrocycles were computed by using the gauge-invariant atomic orbital (GIAO) method.[23−25]

The vertical excitation energies of the complexes were obtained by time dependent density functional theory (TDDFT) at the ground state geometries.[26,27] The nonlinear optical (NLO) properties were evaluated with numerical differentiation of polarizabilities with the finite field (FF) procedure.[28−30] All of the DFT calculations were performed with Gaussian 09 program package.[31]

3. RESULTS AND DISCUSSION

Possible Hückel and Möbius free-base [32]octaphyrins-(1,0,1,0,1,0,1,0) were located by DFT calculations (Scheme 1 and Tables S1 and S2, Supporting Information). Both of them exhibit a twisted conformation with C_1 symmetry. The Hückel and Möbius free-base molecules are nonaromatic in the light of their calculated NICS values of 1.7 and −2.4 ppm, respectively, which are much smaller than the NICS value of benzene (−9.6 to −9.8 ppm).[32−34] To further stabilize the free-base molecules and to modulate the topologies of macrocycles, encapsulations of transition metals Pd and/or Au were implemented. A series of bis-metalated octaphyrins, involving Pd/Pd (a), Pd/Au (b), Au/Pd (c), and Au/Au (d) sets, were built and the interconversions between the stereomers of each set were investigated in detail (Scheme 1 and Figure 1).

3.1. Isomerization Pathways. Six topologically different bis-metalated isomers, three with Hückel pattern (1-H, 4-H, and 6-H) and three Möbius species (2-M, 3-M, and 5-M), were located along the isomerization pathway of each set (Scheme 1, Tables S1 and S2, and Figure S1, Supporting Information). 1-H
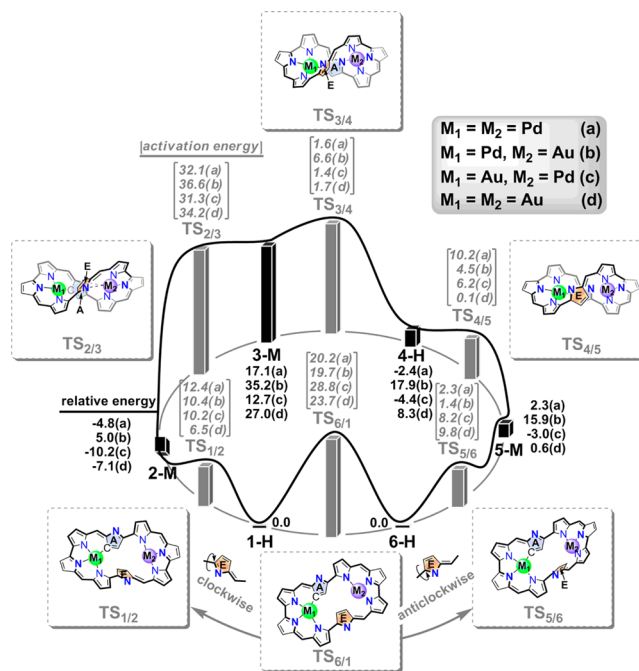
Figure 1. Schematic potential energy diagram along the isomerization reaction pathway; the data are the relative energy (in kcal/mol) of intermediates (1-H, 2-M, 3-M, 4-H, 5-M, and 6-H) and activation energy (in kcal/mol) of transition states (TS$_{1/2}$, TS$_{2/3}$, TS$_{3/4}$, TS$_{4/5}$, TS$_{5/6}$, and TS$_{6/1}$).

is a two-sided Hückel system with two inverted pyrroles, **A** and **E**, in the macrocyclic complex. The metal atom M_1 is bound by three pyrrolic nitrogen atoms and a pyrrolic β-carbon atom, resulting in a nearly planar N3C coordination mode. The coordination bond lengths are less than 2.23 Å. The geometry of N3C coordination core around metal center M_1 is insensitive to the encapsulated metal atoms with M_1 = Pd or Au, as reflected from the nearly identical bond angles spanned at M_1 among the four sets **a−d**. It is clear that the M_1 atom binds stronger with the nitrogen atoms of pyrroles **B** and **C** than that binding with two end points of the hemiporphyrin (i.e., carbon atom of the inverted pyrrole **A** and nitrogen atom of the distant ring **D**). In the following transformations, such a N3C coordination core around M_1 is well preserved at every step; however, the hemiporphyrins with metal atom M_2 present different coordination patterns in various topological complexes.

The central atom M_2 (M_2 = Pd, Au) in **1-H** is only coordinated with three pyrrolic nitrogen atoms with an umbrella-shaped N3 environment. The coordination bond lengths around M_2 are less than 2.38 Å. The uncoordinated pyrrole **E** is very flexible and can be inverted by rotating the adjacent C−C bond. Successively clockwise rotations of ring **E** give rise to a multistep interconversion of the metalated complexes.

In the first step, the rotation of pyrrole **E** by about 31° leads to a Möbius-type local minimum, **2-M**. The activation barriers for this step are calculated to be 6.5−12.4 kcal/mol, implying the facile Hückel−Möbius transition. **2-M** shows a twisted single-sided Möbius topology with an explicit phase change within its p-orbitals. The cross-section of π orbital divides the twisted macrocycle into two roughly planar segments, with each of them capsulizing a metal atom (M_1, M_2 = Pd, Au) in the center. The coordination in left hemiporphyrin of **2-M** still keeps N3C mode regardless of whether Pd or Au atom is bound, but diversity has been found in the right moiety (with M_2 = Pd, Au) for different sets (Scheme 2). When the metal

(3.17 Å) in **2-M** of Pd/Au (**b**) set induces a significant exaltation of more than 10 kcal/mol in relative energy (Figures 1 and S1, Supporting Information). Such an incompact coordination in the right moiety of Pd/Au (**b**) set does not appear to induce distinct charge separation as compared to the electrostatic potential (ESP) with those of other three sets (Scheme 2).

The next step is the rate-determining step of the overall isomerization with an activation energy of no less than 30 kcal/mol. Among the four bis-metalated sets, the Pd/Au (**b**) complex still shows the particularity with the largest activation energy of 36.6 kcal/mol. The transition state, $TS_{2/3}$, is a late transition state in this reaction pathway. The uncoordinated pyrrolic unit **E** leaves the central metal atom M_2 (M_2 = Pd, Au) with the interatomic distance $M_2 \cdots N(\textbf{E})$ longer than 4.10 Å. A $M_2−N(\textbf{A})$ bond forms simultaneously in **3-M** with the bond length shorter than 2.31 Å. As a result, the pyrrolic ring **A**, whose β-C atom has already coordinated with metal atom M_1 (M_1 = Pd, Au), affords the N atom to form the $M_2−N$ bond again. The M_2 (M_2 = Pd, Au) atom in **3-M** hereby presents a nearly planar four-coordinated $M_2−N4$ mode for all four sets. Remote pyrrole **E** serves as a flexible linker between the nearest pyrrolic units and leads to quite smooth figuration of **3-M**. The intermediate **3-M** is calculated to be about 22 and 32 kcal/mol less stable than its precursor, **2-M**, for the sets with M_2 = Pd (**a** and **c**) and Au (**b** and **d**), respectively.

Starting from **3-M**, a successive torsion of the flexible pyrrolic ring **E** gives the second Hückel conformer **4-H**. The transition state $TS_{3/4}$ is an early saddle point with a small barrier of less than 7 kcal/mol. Again, the transition state of Pd/Au (**b**) complex exhibits the largest activation energy (6.6 kcal/mol) among the four sets. The $M_2−N(\textbf{A})$ distances in **4-H** are calculated to be 2.13, 2.10, and 2.16 Å for Pd/Pd (**a**), Pd/Au (**b**), and Au/Pd (**c**) species, respectively, whereas they are a little longer at 2.33 Å for the Au/Au (**d**) set. The different degrees of twisting in molecular backbone around M_2 atom are reflected by inter-ring dihedral between pyrroles **H** and **A**. The N4 coordination geometry of the left moiety of **4-H** is quite similar to that of its precursor, **3-H**.

Further turning of the canted pyrrole **E** yields a new Möbius isomer **5-M**. The M_2 (M_2 = Pd, Au) atom seems to present an umbrella-shaped N3 mode with the $M_2−N$ distances less than 2.22 Å, and the average $N−M_2−N$ bond angle of about 90° around umbrella surface. This step needs to get over 10.2, 4.5, and 6.2 kcal/mol activation barrier for Pd/Pd (**a**), Pd/Au (**b**), and Au/Pd (**c**) sets via transition state $TS_{4/5}$. In contrast, the transition from **4-H** to **5-M** of Au/Au (**d**) complex is almost barrierless with the activation energy of only 0.1 kcal/mol, which benefits from the nearly identical geometries of $TS_{4/5}$ and **4-H** with the negligible difference (of only 1.4°) in relative torsion angle of pyrrole **E** between these two species.

Finally, we reach the last intermediate **6-H** through clockwise rotation of the pyrrole **E** in **5-M** with a torsion angle of about 124°. The potential energy surface (PES) becomes very flat in this step and the barrier is found to be no more than 10 kcal/mol. The flat PES between **4-H** and **6-H** suggests the possibly reversible Hückel-Möbius-Hückel interconversions through **5-M**.

In fact, **6-H** is the enantiomer (mirror image) of **1-H**, which can be identified by their ECD spectra (Figure S2, Supporting Information). The chiral interconversion may occur in one-step by rotating the pyrrole **E** anticlockwise with a barrier of less than 30 kcal/mol through $TS_{6/1}$. For this direct isomerization,

**Scheme 2. Electrostatic Potential (ESP) and Selected Geometric Parameters around Metal Centers of 2-M**
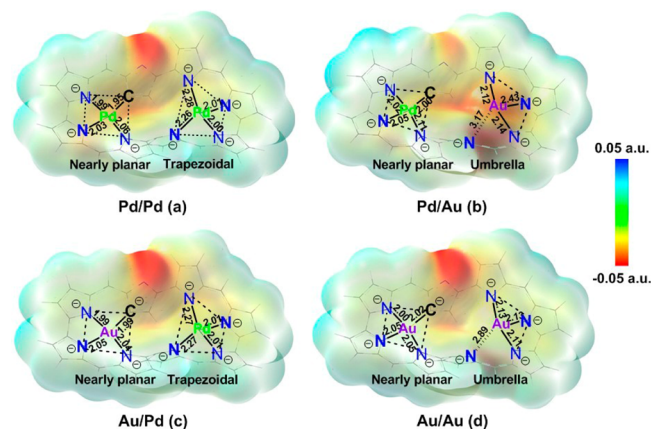
core of right hemiporphyrin is M_2 = Pd atom (**a** and **c** sets), trapezoidal coordination with M_2-N4 mode is the preferred pattern. In contrast, the $Au \cdots N(\textbf{E})$ distances of 3.17 and 2.89 Å in right moiety of Pd/Au (**b**) and Au/Au (**d**) sets are larger than those reported for gold porphyrins (2.08−2.11 Å),[35] exhibiting an umbrella-like N3 coordination with central Au atom in right hemiporphyrin. The longer $Au \cdots N(\textbf{E})$ distance

the smallest activation barrier of 19.7 kcal/mol is presented in Pd/Au (**b**) series, which is different from the more difficult multistep transformation of Pd/Au (**b**) and Au/Au (**d**) complexes with M_2 = Au than those Pd/Pd (**a**) and Au/Pd (**c**) sets with M_2 = Pd. To summarize, there are two alternative ways to realize the chiral isomerization, by twisting the active pyrrole **E** either clockwise (multistep interconversion) or anticlockwise (one-step isomerization): the complexes with M_2 = Au favor the one-step transformation and M_2 = Pd cases prefer the multistep one.

3.2. π-Conjugations in Stationary Points. The structural difference between Hückel (**1-H**, **4-H**, and **6-H**) and Möbius (**2-M**, **3-M**, and **5-M**) topologies of the studied systems lies in the relative orientation of pyrroles **A** and **E** in the macrocycles. For the Möbius systems, the pyrroles **A** and **E** arrayed in a crossed manner with the average tilted angle of 77.7°, whereas they roughly face toward the same direction with the average tilted angle of 29.5° in the Hückel structures.

The difference between Hückel and Möbius topologies is also reflected from the distinct variation of the backbone, as characterized by the extent of inter-ring bond length alternation (BLA, Figure 2a).[36−40] For the **a**–**d** sets, the average BLA values
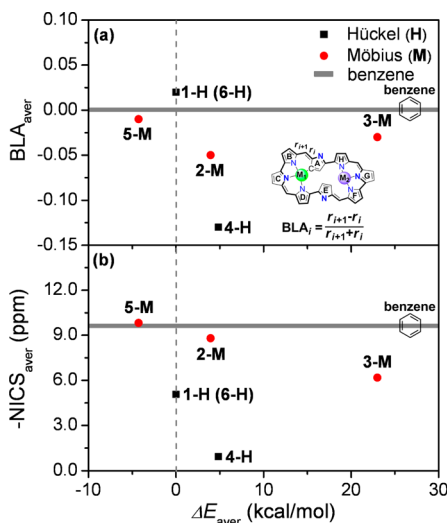

Figure 2. Plot of (a) BLA and (b) NICS values versus the relative energies to **1-H** for various topologies.

of Hückel-type **1-H** (**6-H**) and **4-H** are setting as two ends of 0.02 and −0.13, respectively, whereas the data of Möbius-like **2-M** (−0.05), **3-M** (−0.03), and **5-M** (−0.01) are located in the middle of them. The decreased BLA values of the complexes imply the transition into the quinoid structure on going from **1-H** to **4-H**, passing through the Möbius-type **2-M** and **3-M** (Scheme 1). The reverse quinoid-aromatic transformation from **4-H** to **6-H** via **5-M** is also observed.

The difference in structure of the macrocycles implies the discrepancy in their aromaticity. The NICS is a useful measure in predicting the aromaticity of cyclic systems.[23,25] In this context, we employed GIAO method to calculate the magnetic parameter, NICS value, of the studied bis-metalated octaphyrins. The realization of various macrocyclic topologies is relevant to the aromatic stabilization effect of macrocycles. As shown in Figure 2b, the relative stability of Hückel and Möbius systems parallels their respective NICS values.

For all the studied Möbius bis-metalated complexes (**2-M**, **3-M**, and **5-M**), the NICS values at the center of macrocycles are

considerably negative (Figure 3), characteristic of the aromatic species. The Möbius structures that encapsulate Au atom in the
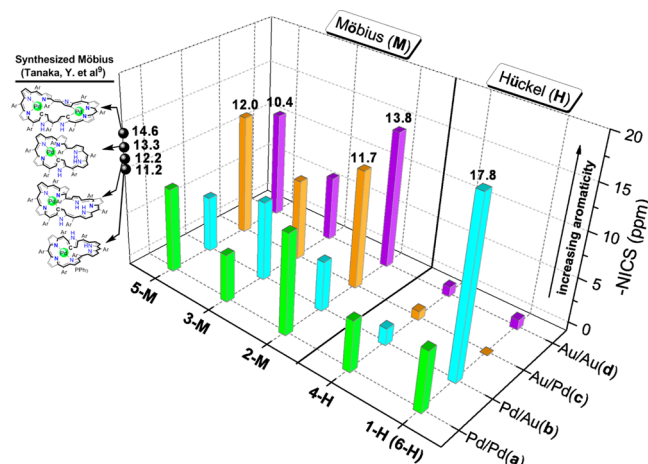
Figure 3. NICS values of bis-metalated [32]octaphyrins-(1,0,1,0,1,0,1,0).

left hemiporphrin (M_1 = Au) always show stronger aromaticity than the complexes with M_1 = Pd. The most striking examples are **2-M** and **5-M**, which even have more negative NICS values than that of benzene (−9.6 to −9.8 ppm). The NICS values of these Möbius systems are comparable to those of the reported Pd-coordinated complexes[9] (−11.2 to −14.6 ppm, see the inset in Figure 3). Some synthesized Möbius-type expanded phyrins with Au atom coordination have also been reported.[15,35,41] The aromaticity of the Au-coordinated complexes predicted here may arouse the interest in preparation of novel macrocycles. It is also interesting to make comparisons between different criteria of aromaticity (based on geometric, energetic, and magnetic properties, respectively). In comparison with other sets of **2-M**, the Pd/Au (**b**) complex exhibits a strong tendency of electron delocalization with the BLA value close to 0. However, the evident bond length equalization and planarity of backbone do not necessarily ensure the enhanced thermodynamic stability of the π-conjugated systems.[6,25] The Pd/Au (**b**) complex of **2-M** is less stable with 5.0 kcal/mol higher in energy than **1-H**. But other sets of **2-M** present much lower energies (Pd/Pd (**a**), −4.8 kcal/mol; Au/Pd (**c**), −10.2 kcal/mol; Au/Au (**d**), −7.1 kcal/mol) than their precursor, **1-H**. In addition, the Pd/Au (**b**) species of **2-M** shows weaker magnetic aromaticity (with the small NICS value of −4.1 ppm) than the other sets (whose NICS values are −9.7 ppm (**a**), −11.7 ppm (**c**), and −13.8 ppm (**d**), respectively). The similar situation has also been observed for **5-M** series. Therefore, the characterization of the aromaticity of the complex macrocyclic systems can not solely rely on a single criterion and comparisons of several indexes were recommended to give a comprehensive understanding of the electron delocalization.[25]

As expected, the Hückel systems present nonaromaticity owing to their 4n π-electron structures. The calculated NICS values of **1-H** (**6-H**) and **4-H** fluctuate around zero for four sets. The results are consistent with the assertion that stronger aromatic characteristics will be observed in 4n π-electron Möbius system than in Hückel system. The only exception is **1-H** of Pd/Au (**b**) set. Despite its Hückel topological, **1-H** of Pd/Au (**b**) set has the largest negative NICS values (−17.8 ppm) of all species, rationalizing the outstanding stability of **1-H** in **b**
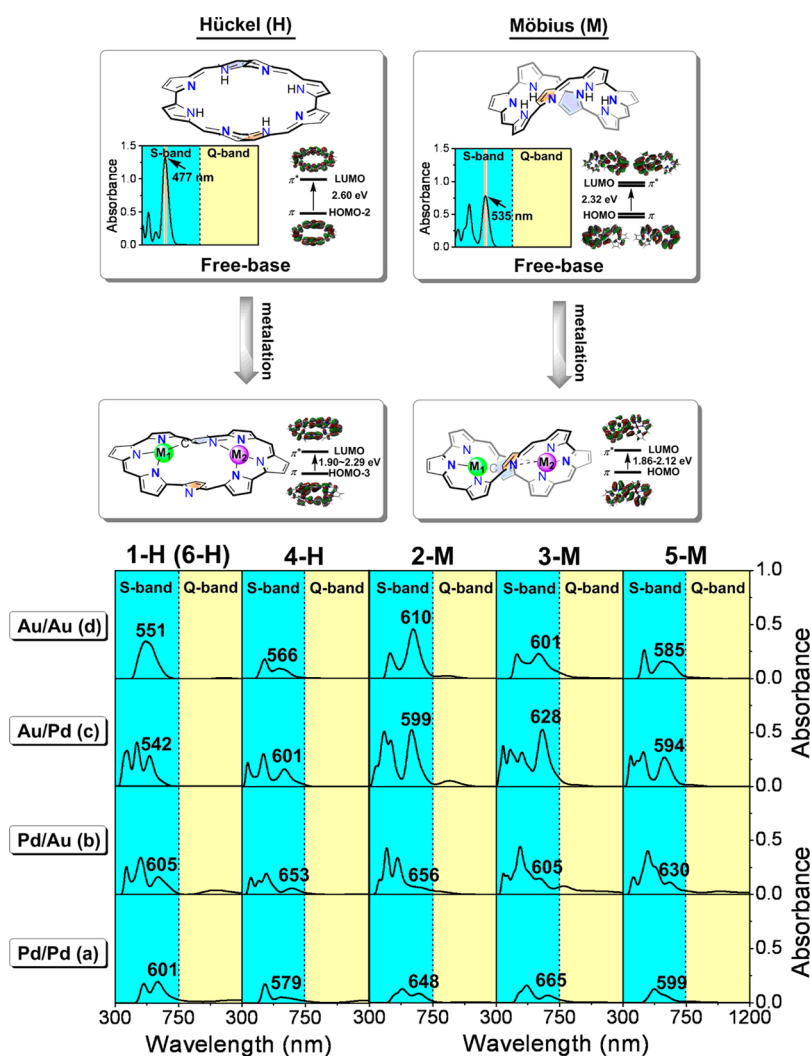
Figure 4. Absorption spectra of free-base and bis-metalated octaphyrins obtained from TDDFT calculations.

species than in other sets. In fact, such a Pd/Au complex of **1-H** has an evident electron delocalization picture with BLA = 0.

3.3. Red-Shift in Soret-Like Bands of UV−vis Spectra. To survey the metalation effect on absorption spectra of the expanded porphyrins, the dipole-allowed vertical transition energies were calculated through TDDFT calculations at B3LYP level (Figure 4). The electronic absorption spectra of free-base rings show strong Soret-like bands for both Hückel (at 348, 406, and 477 nm) and Möbius (at 322, 409, and 535 nm) systems. The main contribution to the lowest excitation energy for free-base Möbius molecule comes from the transition between the highest occupied molecular orbital, HOMO, and the lowest unoccupied molecular orbital, LUMO. Whereas the low-lying excitation for free-base Hückel isomer is featured by HOMO-2 to LUMO transition. All of these transitions correspond to the π bonding to π* antibonding molecular orbital, that is, π→π* mode.
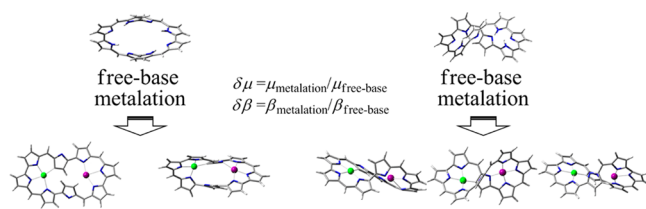
The absorption spectra of metalation products are different from those of free-base ligands. All of the bis-metalated complexes present broad Soret-like bands and the Pd/Au (**b**) sets even show a weak Q-like band. Furthermore, the heterometal-coordinated complexes (i.e., M$_1$ ≠ M$_2$) show stronger and more splitting absorption than the homometal-coordinated ones with M$_1$ = M$_2$. The electronic transitions of bis-metalated complexes also take place primarily from the π

bonding to π* antibonding molecular orbital on peripheral conjugation, called intraligand charge-transfer (ILCT) transition.[42] The introduction of metal ions leads to a significant decrease in the energy gap related to maximum absorption of Soret-like bands. As a result, there are obvious red-shifts of more than 50 nm in the maximum absorption of Soret-like bands of the bis-metalated species in comparison with the free-base molecules. The complexes with M$_1$ = Pd in left moiety present more red-shift than those of M$_1$ = Au (Figures 4 and S3). Furthermore, benefited from the visible planarity, the Hückel systems have stronger overlapping of p-orbitals than Möbius molecules. The more abundant π-conjugation would favor the electronic transition and thus induces a greater red-shift of absorption spectra for Hückel structures than for Möbius isomers.

3.4. Enhancement in Hyperpolarizabilities (β$_0$). The introductions of transition metal atoms also play a crucial role for charge polarization in macrocycles (Table S3, Supporting Information). One can find that the charges in metal atom Pd preserve similar value (0.4−0.5 e) for all sets, either in left or in right moiety. But the charges of Au atom were rather different in different series of **a−d** with the values ranging from 0.2 to 1.2 e. The easy-to-leave 6s^1 electron of Au atom embodied in the electron-withdrawing left moiety may be responsible for the electron redistribution. As a result, the Au/Pd (**c**) and Au/Au

(d) complexes, with Au atom encapsulating in left moiety (M_1 = Au), present higher degree of polarization of the delocalized π-electrons than the other M_1 = Pd systems (Pd/Pd (a) and Pd/Au (b) sets). The positively charged metal centers indicate that charge transfers have occurred upon metalation and more electrons aggregate on the peripheral conjugation after this process. Therefore, large molecular hyperpolarizabilities β_0 are displayed for bis-metalated molecules (Table 1) accompanied

Table 1. Increment in Dipole Moment ($\delta\mu$) and Hyperpolarizability ($\delta\beta$) after Metallation

free-base
metalation

$\delta\mu = \mu_{\text{metalation}}/\mu_{\text{free-base}}$
$\delta\beta = \beta_{\text{metalation}}/\beta_{\text{free-base}}$

free-base
metalation

	1-H (6-H)	4-H	2-M	3-M	5-M
Pd/Pd (a)					
$\delta\mu$	8	8	1	1	1
$\delta\beta$	197	194	16	4	10
Pd/Au (b)					
$\delta\mu$	7	26	1	3	2
$\delta\beta$	39	251	7	11	4
Au/Pd (c)					
$\delta\mu$	6	11	2	1	1
$\delta\beta$	42	30	5	3	1
Au/Au (d)					
$\delta\mu$	3	11	2	1	1
$\delta\beta$	42	75	3	2	2

with the changes in the UV−vis spectra. Especially, the Hückel-type **4-H** of Pd/Au (**b**) complex exhibits the largest increase by about 251 times in hyperpolarizabilities. The result is consistent with the most augment by about 26 times in its dipole moments after metalation.

The increment of hyperpolarizability of Hückel systems is in a much larger extent than that of Möbius structures owing to the breakage of the centrosymmetry and the augment of the planarity during metalation.

4. CONCLUSION

The electronic structures of Hückel and Möbius bis-metalated [32]octaphyrins(1,0,1,0,1,0,1,0) and the chiral interconversions between different macrocyclic configurations have been investigated. The rotation of an uncoordinated pyrrolic ring in the π framework of these complexes leads to the conformational change between Hückel and Möbius topologies with the largest activation energy of no more than 40 kcal/mol. There are two alternative ways to achieve the chiral isomerization of the macrocycles, by twisting the active pyrrolic ring either clockwise (multistep reactions) or anticlockwise (one-step interconversion). The Pd/Au (**b**) and Au/Au (**d**) sets are more difficult to transform in multistep interconvertion reactions than the Pd/Pd (**a**) and Au/Pd (**c**) sets. On the contrary, the Pd/Au (**b**) complex is most facile to undergo one-step transformation between two enantiomers. Some complexes with Au atom encapsulated in left moiety (M_1 = Au) are predicted to be an aromatic macrocycle. The **1-H** complex of

Pd/Au (**b**) complex with a Hückel structure exhibits a strong electron delocalization picture with BLA = 0 and striking aromaticity. The TDDFT results show that the free-base molecules present several sharp Soret-like bands with no Q-like band. But the encapsulations of metal ions induce an appearance of weak Q-like band of adsorption spectra and cause an evident red-shift of the maximum absorption in Soret-like bands. The polarization effect on delocalized π-electrons by the capsulation of metal atoms in macrocycles may increase the molecular hyperpolarizability (β_0), especially for the Hückel systems.

The information of novel topological structures and possible isomerization reactions of the metalated expanded porphrins may shed insight on designs and preparations of new aromatic molecules with unique properties.

■ ASSOCIATED CONTENT

S Supporting Information

DFT optimized Cartesians coordinates of intermediates; computed total energies, the number of imaginary frequency, and imaginary frequencies of stationary points; potential energy diagram along the isomerization reaction pathway; ECD spectra of enantiomers **1-H** and **6-H**; absorption spectra of free-base molecules and bis-metalated species obtained from TDDFT calculations; computed Mulliken charges of metal atoms in intermediates; complete citation for ref 31. This material is available free of charge via the Internet at http://pubs.acs.org.

■ AUTHOR INFORMATION

Corresponding Author
*majing@nju.edu.cn
Notes
The authors declare no competing financial interest.

■ ACKNOWLEDGMENTS

■ REFERENCES

(1) Heilbronner, E. *Tetrahedron Lett.* **1964**, *5*, 1923−1928.
(2) Rzepa, H. S. *Chem. Rev.* **2005**, *105*, 3697−3715 and references therein.
(3) Herges, R. *Chem. Rev.* **2006**, *106*, 4820−4842 and references therein.
(4) Ajami, D.; Oeckler, O.; Simon, A.; Herges, R. *Nature* **2003**, *426*, 819−821.
(5) Ajami, D.; Hess, K.; Köhler, F.; Näther, C.; Oeckler, O.; Simon, A.; Yamamoto, C.; Okamoto, Y.; Herges, R. *Chem.—Eur. J.* **2006**, *12*, 5434−5455.
(6) Castro, C.; Chen, Z.; Wannere, C. S.; Jiao, H.; Karney, W. L.; Mauksch, M.; Puchta, R.; Hommes, N. J. R.; van, E.; Schleyer, P.; von, R. *J. Am. Chem. Soc.* **2005**, *127*, 2425−2432.
(7) Taubert, S.; Sundholm, D.; Pichierri, F. *J. Org. Chem.* **2009**, *74*, 6495−6502.
(8) Park, J. K.; Yoon, Z. S.; Yoon, M.-C.; Kim, K. S.; Mori, S.; Shin, J.-Y.; Osuka, A.; Kim, D. *J. Am. Chem. Soc.* **2008**, *130*, 1824−1825.
(9) Tanaka, Y.; Saito, S.; Mori, S.; Aratani, N.; Shinokubo, H.; Shibata, N.; Higuchi, Y.; Yoon, Z. S.; Kim, K. S.; Noh, S. B.; Park, J. K.;

Kim, D.; Osuka, A. *Angew. Chem.* **2008**, *120*, 693−696; *Angew. Chem., Int. Ed.* **2008**, *47*, 681−684.

(10) Lim, J. M.; Shin, J.-Y.; Tanaka, Y.; Saito, S.; Osuka, A.; Kim, D. *J. Am. Chem. Soc.* **2010**, *132*, 3105−3114.

(11) Tanaka, T.; Sugita, T.; Tokuji, S.; Saito, S.; Osuka, A. *Angew. Chem.* **2010**, *122*, 6769−6771; *Angew. Chem., Int. Ed.* **2010**, *49*, 6619−6621.

(12) Inoue, M.; Yoneda, T.; Youfu, K.; Aratani, N.; Osuka, A. *Chem.—Eur. J.* **2011**, *17*, 9028−9031.

(13) Stępień, M.; Latos-Grażyński, L.; Sprutta, N.; Chwalisz, P.; Szterenberg, L. *Angew. Chem.* **2007**, *119*, 8015−8019; *Angew. Chem., Int. Ed.* **2007**, *46*, 7869−7873.

(14) Stępień, M.; Szyszko, B.; Latos-Grażyński, L. *J. Am. Chem. Soc.* **2010**, *132*, 3140−3152.

(15) Sankar, J.; Mori, S.; Saito, S.; Rath, H.; Suzuki, M.; Inokuma, Y.; Shinokubo, H.; Kim, K. S.; Yoon, Z. S.; Shin, J.-Y.; Lim, J. M.; Matsuzaki, Y.; Matsushita, O.; Muranaka, A.; Kobayashi, N.; Kim, D.; Osuka, A. *J. Am. Chem. Soc.* **2008**, *130*, 13568−13579.

(16) Furuta, H.; Maeda, H.; Osuka, A. *Chem. Commun.* **2002**, 1795−1804.

(17) Toganoh, M.; Furuta, H. *Chem. Commun.* **2012**, *48*, 937−954 and references therein.

(18) Ikeda, S.; Toganoh, M.; Furuta, H. *Inorg. Chem.* **2011**, *50*, 6029−6043.

(19) Fujino, K.; Hirata, Y.; Kawabe, Y.; Morimoto, T.; Srinivasan, A.; Toganoh, M.; Miseki, Y.; Kudo, A.; Furuta, H. *Angew. Chem.* **2011**, *123*, 6987−6991; *Angew. Chem., Int. Ed.* **2011**, *50*, 6855−6859.

(20) Gokulnath, S.; Yamaguchi, K.; Toganoh, M.; Mori, S.; Uno, H.; Furuta, H. *Angew. Chem.* **2011**, *123*, 2350−2354; *Angew. Chem., Int. Ed.* **2011**, *50*, 2302−2306.

(21) Becke, A. D. *J. Chem. Phys.* **1993**, *98*, 1372−1377.

(22) Lee, C.; Ying, W.; Parr, R. G. *Phys. Rev. B* **1988**, *37*, 785−789.

(23) Schleyer, P.; von, R.; Meaerker, C.; Dransfeld, A.; Jiao, H.; Hommes, N. J. R.; van, E. *J. Am. Chem. Soc.* **1996**, *118*, 6317−6318.

(24) Schleyer, P.; von, R.; Jiao, H.; Hommes, N. J. R.; van, E.; Malkin, V. G.; Malkina, O. L. *J. Am. Chem. Soc.* **1997**, *119*, 12669−12670.

(25) Chen, Z.; Wannere, C. S.; Corminboeuf, C.; Puchta, R.; Schleyer, P.; von, R. *Chem. Rev.* **2005**, *105*, 3842−3888 and references therein.

(26) Casida, M. K.; Jamorski, C.; Casida, K. C.; Salahub, D. R. *J. Chem. Phys.* **1998**, *108*, 4439−4449.

(27) Stratmann, R. E.; Scuseria, G. E. *J. Chem. Phys.* **1998**, *109*, 8218−8224.

(28) Cohen, H. D.; Roothaan, C. C. J. *J. Chem. Phys.* **1965**, *43*, 534−539.

(29) Perrin, E.; Prasad, P. N.; Mougenot, P.; Dupuis, M. *J. Chem. Phys.* **1989**, *91*, 4728−4732.

(30) Kurtz, H. A.; Stewart, J. P.; Dieter, K. M. *J. Comput. Chem.* **1990**, *11*, 82−87.

(31) Frisch, M. J.; et al. *Gaussian 09*, revision A.02, Gaussian, Inc.: Wallingford CT, 2009.

(32) Mauksch, M.; Tsogoeva, S. B. *Chem.—Eur. J.* **2010**, *16*, 7843−7851.

(33) Rzepa, H. S. *Chem. Rev.* **2005**, *105*, 3697−3715 and references therein.

(34) Mauksch, M.; Tsogoeva, S. B. *Angew. Chem.* **2009**, *121*, 3003−3007; *Angew. Chem., Int. Ed.* **2009**, *48*, 2959−2963.

(35) Mori, S.; Osuka, A. *J. Am. Chem. Soc.* **2005**, *127*, 8030−8031.

(36) Brédas, J. L. *J. Chem. Phys.* **1985**, *82*, 3808−3811.

(37) Albert, I. D. L.; Marks, T. J.; Ratner, M. A. *J. Phys. Chem.* **1996**, *100*, 9714−9725.

(38) Marder, S. R.; Perry, J. W.; Tiemann, B. G.; Gorman, C. B.; Gilmour, S.; Biddle, S. L.; Bourhill, G. *J. Am. Chem. Soc.* **1993**, *115*, 2524−2526.

(39) Zhang, G.; Ma, J.; Jiang, Y. *Macromolecule* **2003**, *36*, 2130−2140.

(40) Meng, S.; Ma, J. *J. Phys. Chem. B* **2008**, *112*, 4313−4322.

(41) Inoue, M.; Osuka, A. *Angew. Chem.* **2010**, *122*, 9678−9681; *Angew. Chem., Int. Ed.* **2010**, *49*, 9488−9491.

(42) Tessore, F.; Roberto, D.; Ugo, R.; Pizzotti, M. *Inorg. Chem.* **2005**, *44*, 8967−8978.